Simulation and Experimental Research on Dynamics of Low-Pressure Rotor System in Turbofan Engine

Shengxiang Li[1], Chengxue Jin[2], Guang Zhao[1*], Zhiliang Xiong[1], Baopeng Xu[1]

1. Collaborative Innovation Center of Major Machine Manufacturing in Liaoning, Dalian University of Technology, Dalian, P.R. China
2. Seventh thirteen Institute of China Shipbuilding Industry Corporation, hengzhou, P.R. China

Abstract: The support stiffness of low-pressure rotor system (LPRS) in turbofan engine directly influences its rotor dynamics and inherent characteristic. In this paper, the 3D solid finite element model of LPRS is established using Ansys software to conduct grid independent verification and modal analysis. By building Campbell diagram, each order critical speed (CS) of LPRS is calculated, and the variation trend of CS is obtained by changing the dimensionless support stiffness. Finally, static performance test is carried out to verify simulation result. As a result, with the increase of support stiffness, 1st and 2nd order CS increase nonlinearity. 1st order CS is more sensitive to the stiffness of support 3, and 2nd order CS is more sensitive to the stiffness of support 1. Hence, correct choice of support stiffness is significant to rotordynamics design, stability and working speed selection in LPRS.

Keywords: Turbofan Engine; Low-Pressure Rotor System; Critical speed; Support stiffness

1 Introduction

LPRS of the advanced turbofan engine is composed of fan rotor, spline joint and low-pressure turbine (LPT) rotor. LPRS uses spline joint to connect fan rotor and LPT rotor to transmit torque. Past traditional studies on rotor dynamics mostly ignored the effect of support stiffness. However, during the actual flight process, the supports of LPRS in turbofan engine are small support stiffness, high load and large deformation. Hence, the support stiffness has a significant influence on the rotor dynamic characteristics of LPRS, and it is necessary to analysis effect of support stiffness by the finite element model of LPRS. Actual structure of LPRS for turbofan engine is depicted in Fig. 1.

In the past year, many scholars carried out a lot of research works on the modelling and dynamic analysis based on finite element method. CS and modal analysis of hydro-turbine rotor system are taken by using Ansys [1]. Ma [2] built a finite element model of a spur gear pair in mesh is established by considering tip relief. Zhang [3] developed 2D beam element and 3D solid element of rotor system based on ansys, meanwhile, present

* Corresponding author (zhaoguang@dlut.edu.cn)

equivalent-disk method to simplify blades of rotor system. A finite element model including the effects of rotatory inertia, gyroscopic moments, and axial load is developed using the consistent matrix approach [4]. In addition, lots of researches on spline joint are conducted. Barrot et al. [5] presented an analytical study of axial torque transfer in a spline coupling, the axial torque distribution mainly influences the damage related to fretting, without changing the maximum stress coefficient factor at the root of the shaft. Sum et al. [6] discussed a number of key aspects of the 3D finite element (FE) modelling of spline joint for fretting and fatigue assessment. Liu [7] studies the dynamic effects of structure parameters and the external load on the stiffness and contact state of the spline joints with nonlinear finite-element method and experiments. A spline joint model is built to investigate the stiffness mechanical characteristics and affecting factors [8]. Support stiffness of LPRS is significant to CS, hence, selection of the working speed has to know the relationship between the support stiffness and CS accurately.

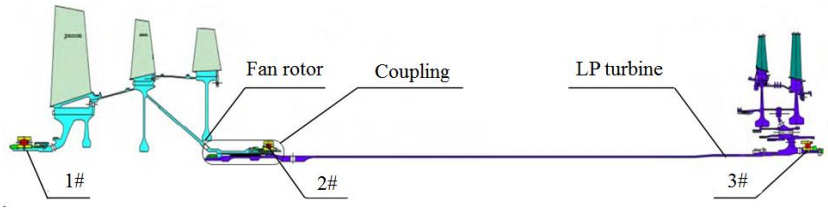

Fig. 1. Actual structure of LPRS for turbofan engine

In addition, some scholars have studied on the stiffness of spline joint and the analytical dynamic modeling. Li et al. [9] study on the meshing stiffness of spline joint of LPRS, and the coupling meshing stiffness under different parameters is obtained. Based on the modified Euler motion equation, Frew and Scheffer [10] calculates the natural frequency and amplitude of rigid rotor that supported by single static pressure gas bearing. A modified pseudo modal vibration mode is used to identify the dynamic characteristics of the rotor-bearing system [11]. For the continuous beam model of rotor system, Lee [12] deduced the analytic solution based on the Non-concomitant system characteristics. Kirkhope et al. [13] deduced the analytical model, the eigenvalue and the analytical solution of the undamped rotor system, and carried out the damping perturbation analysis. Parker [14] deduced the exact solution and the forced vibration response of the rotating disk-shaft system. Erturk et al. [15] use Timoshenko beam model to deduce the analytical model of the spindle rotor, and the frequency response function of a multi section beam is obtained using the flexibility coupling program. Ozsahin et al. [16] have studied the analytical modeling method of the asymmetrical multi-section rotor system. Zhao et al. [17] built an intermediate bearing misalignment model of statically indeterminate rotor system, and it can not only produce the 2X component, but also make the 1X component and CS change.

In summary, the studies on the relationship between the supporting stiffness and the critical speed of LPRS and the sensitivity of the support stiffness with the critical speed are poor. In this paper, since the supports of LPRS in turbofan engine are small support stiffness, high load and CS sensitivity, grid independence verification and modal analysis are carried out based on the Ansys software. The variation trend of the CS in LPRS

ISSN 2572-4975 (Print), 2572-4991 (Online)

is obtained, which changes with the each support dimensionless stiffness. Finally, the dynamic characteristics are analyzed and verified experiment is carried out.

2 Finite element modeling of LPRS

Based on the finite element method and Ansys software, the dynamic model of LPRS is established . By analyzing the grid-independent verification, the meshing mode that can ensure both the calculation accuracy and efficiency is determined.

2.1 Model simplification

The LPRS of a typical turbofan engine is shown in Fig. 1, the simplified structure is shown in Fig. 2. This simplified structure consists of three supports, fan rotor and LPT rotor. Because the spline joint with cylindrical positioning on both ends, it can be approximated as a rigid connection. From left to right in Fig. 2 are the fan rotor, spline joint and LPT rotor. Three supports of LPRS are named as respectively support 1, support 2 and support 3.

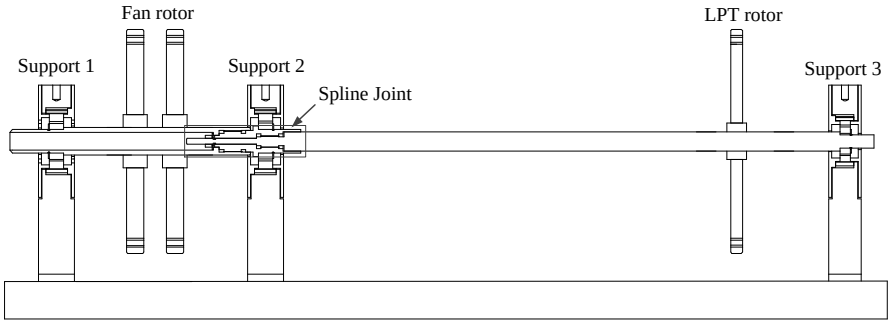

Fig. 2. Simplify structure of LPRS

2.2 3D solid finite element model

As shown in Fig. 3, the finite element solid model is established based on simplified model parameters of LPRS, which adopt the integrated structure, and we do not consider the impact of the contact surface in spline joint. The material constants of LPRS are shown in Table 1. The support structure of LPRS includes rolling bearing, squirrel cage and elastic ring. As shown in Table 2, we obtained the actual support stiffness of each support by finite element static structural analysis.

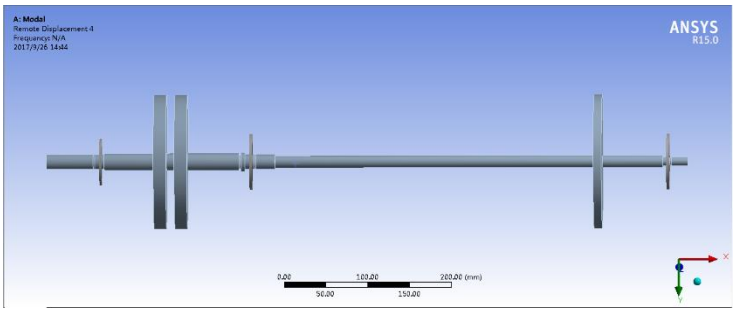

Fig. 3. 3D solid finite element model of low pressure rotor-support system

Table 1. Material parameters

Modulus of elasticity (GPa)	Density (Kg/m^3)	Material damping	Poisson ratio
200.0	7850.0	2×10^{-5}	0.3

Table 2. Support stiffness

Number of support	Support 1	Support 2	Support 3
Support stiffness (MN/m)	1.17	5.96	1.15

The 3D model of each component in LPRS is established by Solidworks software and then import into Ansys software for meshing. The solid element is Solid45 element. After the meshing, the finite element model consists of 44423 nodes and 16160 elements.

In order to verify the independence of the grid, the natural frequencies of the rotor system with the case of grids 1 and 2 are calculated respectively (Table 3). The comparison results are shown in Table 4. Since the two errors are extremely small, the number of grid 1 has reached the requirement, and the impact on the analysis results can be ignored, so the grid 1 is used for calculation and analysis.

Table 3. Mesh parameters

Grid 1	Nodes	16431
	elements	8565
Grid 2	Nodes	49229
	elements	28044

Table 4. Mesh verification results

Modal frequency	1st	2nd	3rd	4th	5th	6th
Grid 1(Hz)	75.1	80.9	120.9	126.7	220.4	261.7
Grid 2(Hz)	74.9	80.8	120.8	126.5	219.8	261.3
Error (%)	0.24	0.22	0.17	0.18	0.29	0.15

ISSN 2572-4975 (Print), 2572-4991 (Online)

3 Modal analysis of LPRS

In this section, we make modal analysis by using the meshing solid model in section 2 to get the first three order modes of LPRS. By drawing Campbell diagram, each order CSs of LPRS are calculated. By calculating the CS of LPRS with different dimensionless support stiffness, the sensitivity of LPRS to the variation of each support stiffness is analyzed.

3.1 Mode shape of LPRS

We set the rotating speed at 3000rpm, consider the gyroscopic effect, the first three order modes are shown in Fig. 4. Since support 2 and support 3 have a large span, the 1st and 3rd order mode is the bending vibration at the LPT side. 2nd order mode is the bending mode of the fan side.

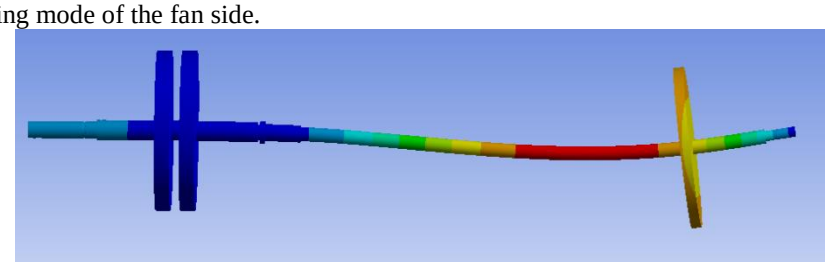

(a) 1st order

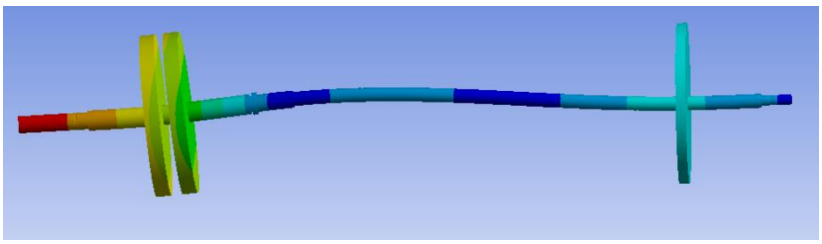

(b) 2nd order

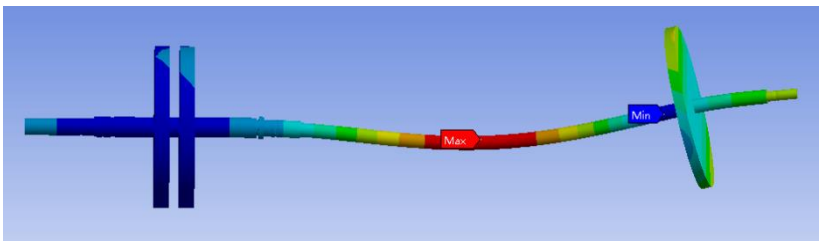

(c) 3rd order

Fig. 4. Mode shapes of LPRS

The vibration results show that the deformation of LPT in the 1st and 3rd modes of LPRS is the largest, which indicates that LPT are more sensitive to the 1st and 3rd modes. The deformation of 2nd order mode is mainly in the fan disk, which indicates that 2nd order mode is more sensitive to the fan disk. In section 3.3, the fact that CS changes with the support stiffness also proves this. Therefore, under the actual operating conditions, when cross the 1st and 3rd order CSs, the vibration response of LPT is the main vibration reason, should pay more attention to avoid exceeding the vibration margin, similarly, when cross 2nd order CS, the response of the fan disk vibration should pay more attention.

3.2 Campbell diagram and critical speed

To obtain the CS of LPRS, the Campbell diagram needs to be drawn by Ansys finite element analysis. The precession frequency corresponding to multiple values of the rotational frequency need to be obtained. Therefore, set the rotational speed at 0, 5000, 10000 and 20000 rpm, respectively. After performing multiple modal solutions, the data is shown in Table 5, and the Campbell diagram is shown in Fig 5.

Table 5. Modal frequency at each speed

Rotational speed (rpm)	0	5000	10000	20000	Critical speed
1st reverse (Hz)	78.1	72.9	67.2	60.5	4413.4
1st positive (Hz)	78.2	82.6	86.3	91.9	5005.3
2nd reverse (Hz)	123.8	119.1	114.7	106.4	7038.2
2nd positive (Hz)	123.8	128.7	133.7	144.1	7893.1
3rd reverse (Hz)	239.6	209.2	186.4	157.8	11010.1
3rd positive (Hz)	239.6	278.1	324.3	435.9	NONE

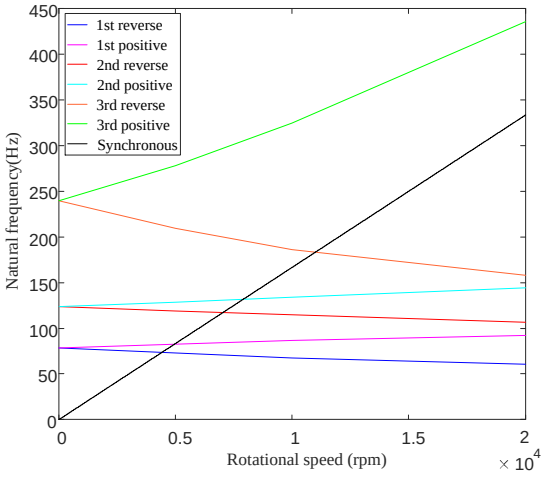

Fig. 5. Campbell diagram of LPRS

ISSN 2572-4975 (Print), 2572-4991 (Online)

As shown in Fig. 5, the *x*-axis is the rotational speed and the *y*-axis is the natural frequency. The curves are respectively 1st order reverse, 1st order positive, 2nd order anti-reverse, 2nd order positive, 3rd-order reverse and the 3rd order positive. The straight line from the origin point is synchronous excitation line. Due to the gyroscopic effect, the reverse precession decreases with the increase of the rotational speed, while the positive precession increases with the increase of the rotational speed.

The excitation speed corresponding to the intersection of the straight line and each frequency curve is the CS. When calculates the CS, only considers synchronous forward whirling, because under the actual rotor operation, due to unbalanced excitation force, the rotor will make synchronous positive whorl, the so-called CS, generally refers to the synchronous forward whirling of the CS.

We can obtain by Fig. 5 that first two orders CSs are 5000.34rpm and 7893.13rpm. It can be seen that when the rotor parameters and support stiffness are Table 1 and Table 2, respectively, working speed of LPRS should avoid the first two orders CSs, and try to make minimum rotational speed higher than 1st order CS, and the maximum speed is lower than 2nd order CS.

3.3 Effect of support dimensionless stiffness

In order to study the effect of support stiffness on the rotor system stability, this section analyzes the sensitivity of supports. By changing the dimensionless support stiffness, the curve of the CS of the system with the support stiffness is obtained.

Chang the dimensionless support stiffness of the support 1, the change of the CS of the system with the support stiffness of the support 1 is obtained as shown in Fig. 6. The results show that 1st order CS increases with the support stiffness of support 1 when the dimensionless support stiffness of support 1 is less than 1. When the support stiffness of support 1 is larger than 1, 1st order CS tends to be steady. The 2nd order CS increases rapidly with the support stiffness of the support 1.

1st order and 2nd order CSs increase 3.0% and 99.2% respectively with support stiffness of the support 1. It can be seen that the support stiffness of the support 1 has a great influence on the 2nd order CS, because the 1st order mode changes most frequently is the LPT side and 2nd order mode deformation is the fan side (Fig. 4). Therefore, increasing the support stiffness of the support 1 is bound to a greater impact on 2nd order CS.

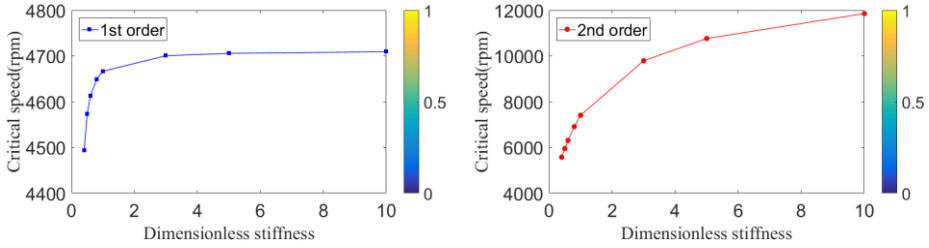

(a) 1st order (b) 2nd order

Fig. 6. CSs versus dimensionless stiffness of support 1

Increase the support stiffness of support 3, the CS with the support dimensionless stiffness is shown in Fig. 7. The results show that 1st order CS of LPRS increases with the support stiffness of support 3 and increases by 12.4%. The 2nd order CS of rotor bearing system increases slightly with the support stiffness of support 3 and increases by only 0.2 %. Since the support 3 is located on the side of the turbine disk, the support stiffness has a great influence on the 1st order CS of the rotor bearing system. Figure 4 shows that the support stiffness of the support 3 is more sensitive to the 1st order CS.

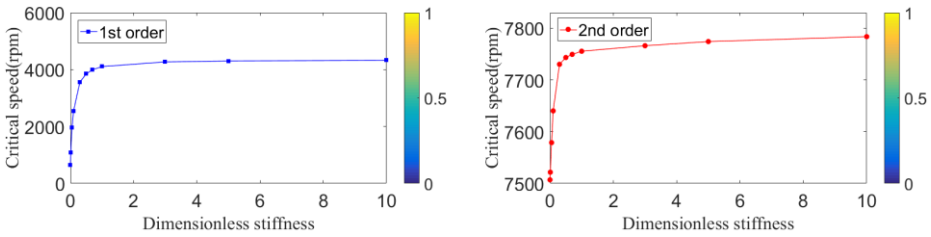

(a) 1st order (b) 2nd order

Fig. 7. CSs versus dimensionless stiffness of support 3

From the results of Figs. 6-7, it is found that the influence of support 1 and 3 on the CS of LPRS is quite different. Therefore, considering the support stiffness of support 1 and support 3 simultaneously, the change of CS with the support stiffness is obtained as Fig. 8 shows. Among them, 1st order CS increases 32.5%, and 2nd order CS increases 101.4%. In contrast, the 1st order CS slowly increases with increase of support stiffness of support 1 and support 3, whereas 2nd order CS increases significantly with increase of support stiffness of support 1 and support 3. In addition, since the support stiffness of the support 2 in LPRS is very high, the influence on the CS is smaller than the remaining two supports, and the details are not described here again.

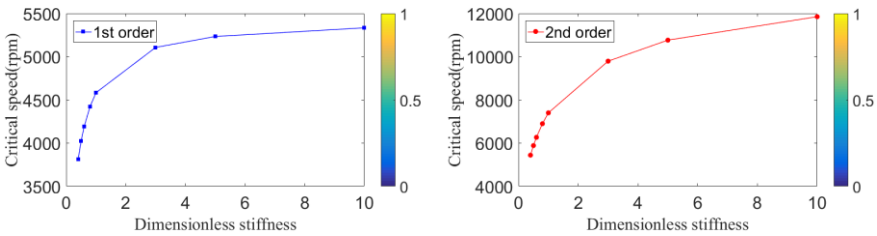

(a) 1st order (b) 2nd order

Fig. 8. CSs versus dimensionless stiffness of support 1 & support 3

In summary, according to Figs. 6-8, the support stiffness of support 1 has a significant influence on 2nd order CS, and support 3 has a great influence on the 1st order CS. In the vibration mode, the deformation of the 1st and 3rd orders mode shapes is the largest in the LPT side. It can be seen that the 1st and 3rd order CSs are more sensitive

 ISSN 2572-4975 (Print), 2572-4991 (Online)

to (i.e. support 3). Similarly, 2nd order mode has the maximum deformation in the fan side, so 2nd order CS is more sensitive to the stiffness variation of the fan (i.e. support 1). Meanwhile, the stiffness of support 1 and support 3 is increased, and the 1st and 2nd CSs of LPRS increase significantly. Therefore, in the actual design of turbofan engine, support stiffness of the CS and stability of the system plays a crucial role, we should choose a reasonable support stiffness and support structure.

Table 6. 1st and 2nd order CS increase rate versus support stiffness

Critical speed	Increase rate of 1st order	Increase rate of 2nd order
Support 1	3%	99.2%
Support 3	12.4%	0.2%
Support 1&Support 3	32.5%	101.4%

4 Experimental test of LPRS

4.1 Introduction of experimental setup

Figure 9 shows the LPRS of turbofan engine simulation experimental setup. This device has three-support structure, including LPT rotor and fan rotor, connected by the spline joint. Membrane coupling are used to connect the motor to the experimental rotor. Each bearing outer ring contains a squirrel-cage and elastic ring, to achieve elastic support. The experimental setup is composed of drive system, LPRS and signal acquisition system.

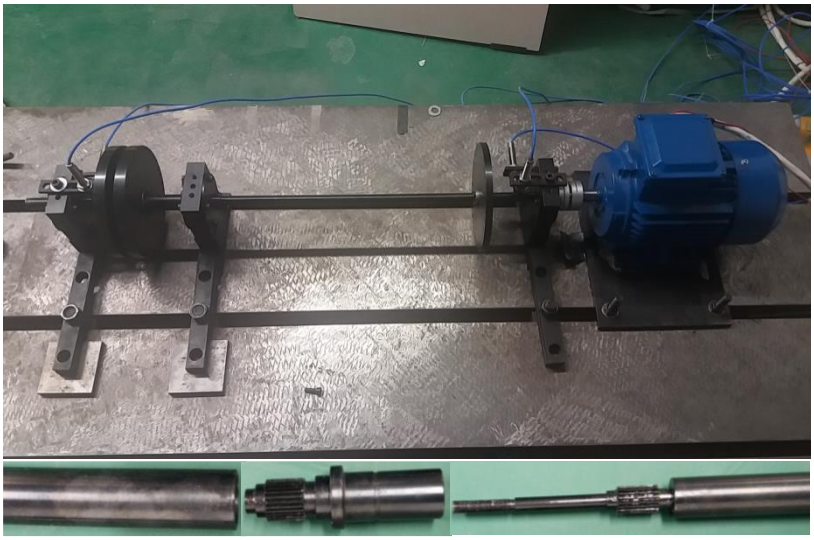

Fig. 9. Photos of LPRS and spline joint

As shown in Fig. 10, signal acquisition system consists of eddy current displacement sensor, information collecting set, preamplifier, and industrial computer. DASP software is used to analysis test results, four eddy current displacement sensors are measured at both ends of the support at the horizontal and vertical vibration displacement, the sensors layout shown in Fig. 10b, we use the frequency changer to adjust the motor to change the rotational speed.

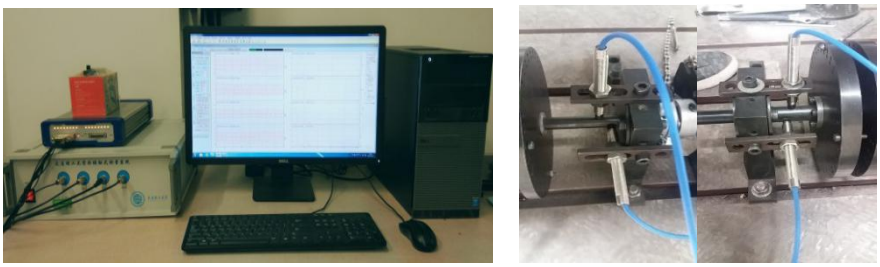

(a) Signal acquisition system (b) Sensors layout

Fig. 10. Photos of signal acquisition system and sensors layout

4.2 Static performance test

In order to analyze the experimental results, we define the eddy current sensor near the motor side of the horizontal and vertical measuring points for the 1*x* and 1*y*, the other side of the eddy current sensor horizontal and vertical measuring points for 2*x* and 2*y*. Hit each disk with a force hammer, the time-domain and FFT is shown in Fig. 11. The 1st order natural frequency of LPRS is 80Hz, and 2nd order is 116.3Hz. Comparing the simulation results, CS results contrast is shown in Table 7

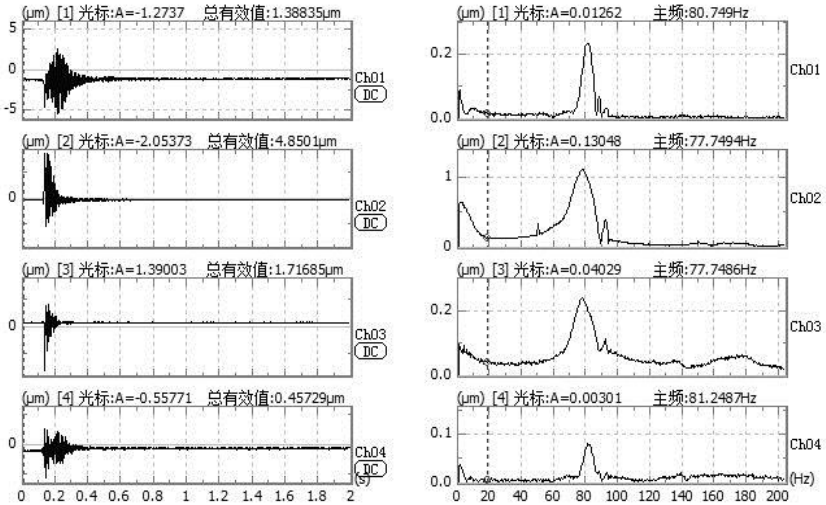

Fig. 11. Time domain and FFT of four sensors

ISSN 2572-4975 (Print), 2572-4991 (Online)

Table 7. Comparison of CS results

Critical speed	1st order /rpm	2nd order /rpm
Static performance test	4800.00	6978.45
Simulation	5005.34	7893.13
Error	4.1%	11.6%

According to the results of Table 7, we can see that the errors of the 1st and 2nd order are 4.1% and 11.6% respectively. The main reason is that due to the complex structure and many influencing factors of the actual LPRS support structure, it is difficult to accurately obtain the support stiffness, which leads to the calculation error of the CS, and we do not consider the influence of the nonlinear stiffness of the contact surface of the spline joint, also resulting in the calculation error.

5 Conclusions

In this paper, since the supports of LPRS in turbofan engine are small support stiffness, high load and CS sensitivity. By building the 3D solid finite element model of LPRS, the dynamic characteristics of LPRS are calculated. Finally, the static performance test is carried out to verify the results of simulation. The main conclusions are as follows:

(1) The result of vibration mode shows that 1st and 3rd order modes of LPRS are sensitive to deformation of LPT side, and 2nd order mode is more sensitive to deformation of fan side. Hence, under actual conditions, the deformation of LPT is the main reason of vibration at 1st and 3rd order CSs, Attention should be paid to keeping the vibration of LPT side within a reasonable range. At same way, more attention should be paid to the vibration of the fan side at 2nd order CS.

(2) With the increase of each support stiffness, 1# support stiffness makes the 1st order CS increase 3.0% and the 2nd order CS increase 99.2%; 3# support stiffness makes the 1st order CS increase 12.4% and the 2nd order CS increase only 0.2%; 1# &3# support stiffness makes the 1st order CS increase 32.5% and the 2nd order CS increase 101.4%. In general, 1st and 2nd order CSs increase nonlinearity with support stiffness, 1st order CS is more sensitive to support 3, and 2nd order CS is more sensitive to support 1, and it is same as the results of the mode shape.

(3) The correct selection of support stiffness is very important for the design, stability and working speed determination of aero-engine rotor system, so support structure should be chosen reasonably. This paper provides a reference for selection of the support stiffness and critical speed of LPRS in turbofan engine.

Acknowledgement

This work is supported by the National Natural Science Foundation of China (Grant No.11672053 and 11472068).

References

1. B. Bai, L. Zhang, T. Guo, C. Liu, Analysis of Dynamic Characteristics of the Main Shaft System in a Hydro-turbine Based on ANSYS, ***Procedia Engineering*** 31 (2012) 654-658.
2. H. Ma, J. Yang, R. Song, S. Zhang, B. Wen, Effects of Tip Relief on Vibration Responses of a Geared Rotor System, ***Proceedings of the Institution of Mechanical Engineers Part C Journal of Mechanical Engineering Science***, 228 (2014) 1132-1154.
3. L. Zhang, J. Hong, Y. H. Ma, Modeling method and vibration characteristics of aero-engine rotor system, ***Journal of Beijing University of Aeronautics and Astronautics***, 39 (2013) 148-153.
4. H. D. Nelson, J. M. Mcvaugh, The Dynamics of Rotor-Bearing Systems Using Finite Elements, ***Journal of Engineering for Industry***, 98 (1976) 593.
5. A. Barrot, M. Paredes, M. Sartor, Extended equations of load distribution in the axial direction in a spline coupling, ***Engineering Failure Analysis***, 16 (2009) 200-211.
6. W. S. Sum, S. B. Leen, E. J. Williams, R. Sabesan, I. R. McColl, Efficient Finite Element Modelling For Complex Shaft Couplings Under Non-Symmetric Loading, ***Journal of Strain Analysis for Engineering Design***, 40 (2005) 655-673.
7. S. Liu, Y. Ma, D. Zhang, J. Hong, Studies on dynamic characteristics of the joint in the aero-engine rotor system, ***Mechanical Systems & Signal Processing*** 29 (2012) 120-136.
8. Q. Zhang, W. Li, Z. Liang, J. Hong, Study on the Stiffness Loss and its Affecting Factors of the Spline Joint Used in Rotor Systems, ***ASME Turbo Expo 2014: Turbine Technical Conference and Exposition American Society of Mechanical Engineers***, 2014, Vol 7a, (2014).
9. J. Li, Y. Ma, J. Hong, Dynamic Design Method of Spline Joint Structure for Rotor System, ***Aeroengine***, 35 (2009) 36-39.
10. D. A. Frew, C. Scheffer, Numerical modelling of a high-speed rigid rotor in a single-aerostatic bearing using modified Euler equations of motion, ***Mechanical Systems & Signal Processing***, 22 (2008) 133-154.
11. Y. S. Chen, Y. D. Cheng, T. Yang, K. L. Koai, Accurate identification of the frequency response functions for the rotor–bearing–foundation system using the modified pseudo mode shape method, ***Journal of Sound and Vibration***, 329 (2010) 644-658.
12. C. W. Lee, Y. G. Jei, Modal analysis of continuous rotor-bearing systems, ***Journal of Sound and Vibration***, 126 (1988) 345-361.
13. W. Wang, J. Kirkhope, New eigensolutions and modal analysis for gyroscopic/rotor systems, part 1: undamped systems, ***Journal of Sound and Vibration***, 175 (1994) 159-170.
14. R. G. Parker, P. J. Sathe, Exact solutions for the free and forced vibration of a rotating disk-spindle system, ***Journal of Sound and Vibration***, 223 (1999) 445-465.
15. A. Ertürk, H.N. Özgüven, E. Budak, Analytical modeling of spindle–tool dynamics on machine tools using Timoshenko beam model and receptance coupling for the prediction of tool point FRF, ***International Journal of Machine Tools & Manufacture***, 46 (2006) 1901-1912.
16. O. Özşahin, H.N. Özgüven, E. Budak, Analytical modeling of asymmetric multi-segment rotor – bearing systems with Timoshenko beam model including gyroscopic moments, ***Computers & Structures***, 144 (2014) 119-126.
17. G. Zhao, S. Li, Y. Zhang, Z. Xiong, Q. Han, Analytical Dynamic Model of Statically Indeterminate Rotor System and Misalignment, ***ASME Turbo Expo 2017: Turbomachinery Technical Conference and Exposition***, 2017, Vol 1T, (2017).

 ISSN 2572-4975 (Print), 2572-4991 (Online)